Lowland Technology International 2016; 18 (3): 197-208
International Association of Lowland Technology (IALT): ISSN 1344-9656

Research Paper

Behaviors of soil cement columns and stiffened soil cement column wall in shallow excavation

I. Meepon [1], P. Voottipruex [2] and P. Jamsawang [3]

ARTICLE INFORMATION

Article history:

Received: 20 August, 2016
Received in revised form: 27 September, 2016
Accepted: 14 November, 2016
Publish on: 28 December, 2016

Keywords:

Soil cement column
Jet grouting
Horizontal displacement
Effective thickness

ABSTRACT

This research aims to presents results of laboratory investigations on cement-admixed clay and full scale of soil cement column (SCC) walls and stiffened soil cement column (SSCC) walls of 60 cm in diameter and 8 m depth constructed in soft Bangkok clay in various forms. There are five types of wall namely, type A: three row of soil cement column, type B: two rows of soil cement column, type C: one row of cement column inserted with steel H-beam in each column, type D: one row of soil cement column alternately inserted with H-beam, and type E: one row of soil cement column without reinforcement. The shallow excavation was conducted step by step with depth increment 1 m to 5 meter. Immediately after excavation; it can be observed from inclinometer that the horizontal movement of all type of wall exhibited slightly different. However, one day after excavation; the type A wall exhibited minimum movement of 6.37 mm; follow by type B wall with movement of 15.76 mm, and type C wall with movement of 22.37 mm. The maximum movement was observed from type D wall with movement of 51.99 mm while the type E wall failed one day after excavation. Alternate H-shaped steel reinforcement in the soil cement wall resisted bending moment due to lateral earth pressure up to a certain excavation depth. Beyond this depth the bending moment decreased, and the horizontal movement of the wall exhibited rigid body translation mode. The SSCC wall resisted bending moment due to lateral earth pressure through the embedded H-shaped steel in the soil cement column. Strain values indicated that the horizontal force was transferred to the embedded steel. Horizontal movement at the pile cap increased as the horizontal force increased. The SSCC continuously resisted the horizontal force through the embedded H-shaped steel, and a linear relationship between horizontal load and horizontal displacement was observed.

[1] Doctoral student, Dept. of Teacher Training in Civil Engineering King Mongkut's University of Technology North Bangkok, THAILAND, ittipon.kmutnb@gmail.com
[2] Assoc. Prof. Dept. of Teacher Training in Civil Engineering, King Mongkut's University of Technology North Bangkok, THAILAND, pnv@kmutnb.ac.th
[3] Asst. Prof. Dept. of Civil Engineering King Mongkut's University of Technology North Bangkok, THAILAND, pitthaya@kmutnb.ac.th
Note: Discussion on this paper is open until June 2017

1. Introduction

Over 20 years ago, the construction of retaining concrete walls or steel sheet pile walls in Scandinavia, Japan, Germany, America and Asian countries was replaced with soil cement column (SCC) jet grouting (Jamsawang et al., 2015; Boathong et al., 2014). Using SSC reduces imported materials and products that require a lot of energy in the production process. Most of the excavation works in and the vicinity of Bangkok are shallow, however, the protection systems required are almost similar to deep excavations. Excavation in limited spaces requires proper protection. Therefore, an SCC wall can be used as an alternative system for shallow excavation (Modoni et al., 2012). The disadvantage of an SCC wall as a retaining structure is the low bending resistance owing to the brittleness of SCC. To enhance the bending resistance, H-shaped steel was embedded (Jamsawang et al., 2015).

Bergado et al. (1996) stated that the main factors influencing the hardness of soil cement were the type of cement, cement content, curing time, soil type, curing temperature, minerals in the soil, and soil pH. To improve the engineering properties of soft soil, natural soil can be mixed with binders in the form of cement slurry or lime, or powdered cement (Porbaha et al., 1999). Treated soft soil becomes a solid body of soil cement due to pozzolanic reaction. The SCC can be overlapped and formed in various patterns. It described a technique for soil improvement using cement slurry or cement powder. The natural soil mixes with the binder. The engineering properties of the soil improved and the soil condition changed from loose to solid state. A soil cement column is one type of soil improvement that can be applied for earth retaining structures and installed in various forms, including some reinforcement in the column such as timber or steel. Wang et al. (2007) studied the interaction between small H-shaped steel reinforcement and soil cement retaining walls. The H-shaped steel reinforcement exhibited an effect on the bending stiffness of the soil cement retaining wall before and after cracking occurred. To study the performance and application of soil cement mixing (SCM), Mun et al. (2012) conducted field experiments and a 3D finite element method was used to study the stability of a soil cement mixing wall. Related research was reviewed and the parameters obtained and used in this study included the size of column, column overlapping, column embedment, and column strength. Voottipruex et al. (2010) studied the numerical simulation of deep cement mixing (DCM) and stiffened deep cement mixing (SDCM) under both axial and horizontal loads. SDCM refers to soil cement columns reinforced with concrete piles and the embankment was constructed over the SCDM in the field. Behaviors of SCDM and DCM under axial and horizontal loads were studied, and compared to numerical modeling using the 3D finite element program PLAXIS 3D. The parameters obtained for numerical modeling for DCM and SCDM included clay cement cohesion and clay cement modulus which were 300 kPa (C_{DCM}) and 60,000 kPa (E_{DCM}) for DCM, and 200 kPa (C_{SDCM}) and 40,000 kPa (E_{SDCM}) for SDCM, respectively. The numerical simulation of reinforced soil cement columns revealed that as the length ratio between the concrete core and deep cement mixing (L_{core} / L_{DCM}) increased, the bearing capacity of the soil cement also increased. On the other hand, the cross-sectional area ratio (A_{core} / A_{DCM}) had little effect on the strength of the axial bearing capacity. The increment of cross-sectional area ratio (A_{core} / A_{DCM}) had a significant effect on horizontal force resistance, while the length ratio (L_{core} / L_{DCM}) had little effect on horizontal resistance if the length of concrete core was longer than 3.5 m. Moreover, both tensile strength of deep cement mixing (T_{DCM}) and tensile strength of concrete core (T_{core}) significantly contributed to the horizontal resistance of the soil cement column. Simulation results showed that the tensile strength of the concrete core (T_{core}) and tensile strength of deep cement mixing (T_{DCM}) were 5,000 kPa and 50 kPa, respectively.

This research investigated the performance of soil cement column (SCC) and stiffened soil cement column (SSCC) walls applied for shallow excavation. The test plot was located in Wang Noi District, Ayutthaya Province, Thailand. Five types of retaining wall with length of 4.6 m and depth of 8 m were constructed as shown in **Fig. 9.** In the type C wall, H-shaped steel of 6 m length was embedded into every soil cement column, while in the type D wall, H-shaped steel was alternatively embedded into the soil columns. After 28 days of soil cement wall construction, shallow excavations were made in steps of 1 m depth to 5 m depth. At every 1 m of excavation, the lateral movement of the soil cement wall was measured by an inclinometer and the strain on the H-shaped steel surface was detected by a strain gauge. At the end of excavation to 5 m depth, the test results were collected and the effect of wall thickness on horizontal resistance was investigated for each type of soil cement wall. The soil cement study mainly concerned the bearing capacity or effectiveness of the length ratio of reinforcement material. The behavior of shaped steel reinforcement affixed with strain gauges has never been previously determined. The findings from this study can benefit the applications of shallow excavation using soil cement columns.

2. Soil profile, soil cement wall construction and instrumentation

The research was conducted in test plots at Wang Noi District, Ayutthaya Province, Thailand. Soil properties obtained from subsurface investigation and soil boring are shown in **Figs. 1** and **2**, which include the unit weight, natural water content (w_n), liquid limit (LL), plastic limit (PL). Soft clay was found from the surface down to 8 m depth, underlain by 2 m of stiff grey clay followed by 3 m of very stiff brown clay. The groundwater table was located at a depth of 0.30 m below the ground surface. According to the Unified Soil Classification System (USCS), the uppermost layer was classified as high plasticity clay (CH).

The soil cement column was installed using a jet grouting method with pressure of 25 MPa to form various types of retaining wall at 4.6 m length. Each column was 60 cm in diameter and depth of 8 m. The water cement ratio of the cement slurry was 1.5, and the cement content was 240 kg/m^3 of natural soil as shown in **Table 1**. The soil cement column was installed with a 10 cm overlap and H-shaped steel 200 x 200 mm was inserted in wall type C and type D. To measure the bending moment that occurred during excavation in the H-shaped steel, strain gauges were affixed on the steel surface as shown in **Fig. 3**.

To measure the horizontal movement of excavation work an inclinometer was installed through the soil cement column 11mbelow and 1m extrude from the ground surface, respectively. Tip of Inclinometer tube should be embedded in the stiff clay layer in order to prevent the simultaneous movement of cement column and inclinometer tube. Inclinometer tube with a length of 12 m was inserted into cement column 28 days after construction while surface settlement plates were installed behind the soil cement walls as shown in **Figs. 10** and **11**.

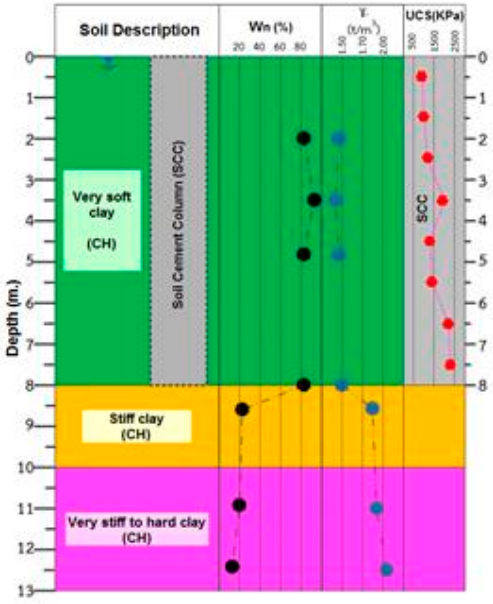

Fig. 1. Soil boring log.

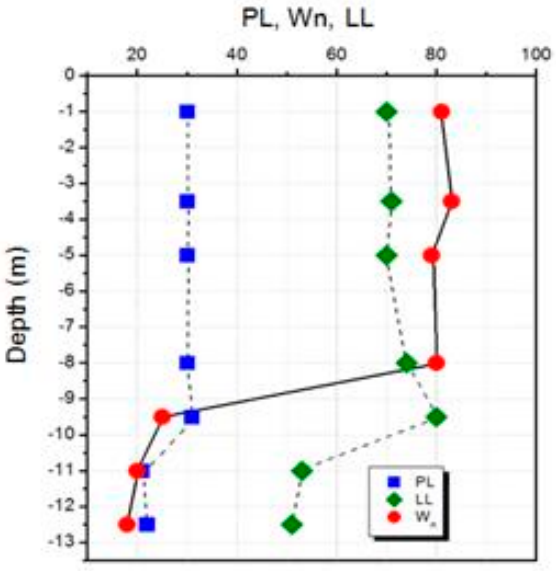

Fig. 2. Atterberg limits of soil.

3. Laboratory Tests

3.1 Unconfined compressive strength test of the soil cement

One of the techniques of improving thick deposit of soft ground is deep mixing method (DDM). In DMM, the chemical agents which are either powder or slurries of lime or cement are mixed into the ground to form column of soil cement pile. When cured these columns of improved soil would stabilize and harden (Bergado et al., 2004).Typically, cement content ranges from 10 to 30% while the volumetric binder content ranges from 150 to

Table 1. Detail of soil cement jet grouting.

Details	Quantity
Diameter, mm	600
Jet grouting depth, m	8.00
Pressure, MPa	25
Nozzle diameter, mm^2	7.76
Lifting speed, mm/s	15
Cement content, kg/m^3	240
W:C ratio	1.5

300 kg/m^3 (Han, 2015). To investigate the strength development of the soil cement with various cement content in laboratory, specimens were prepared by mixing soft clay with cement and cast in cylindrical molds with diameter 50 mm and height 100 mm. The cement content ranged from 10, 15, 20, 25, and 30%, respectively while water content (C_w) was 110%. Unconfined compressive strength testing was conducted 28 days after curing, and the results revealed that unconfined compressive strength increased as the cement content (Aw) increased from 290.40, 450.20, 612.20, 673.60, and 844.30 kPa, respectively. Unconfined compressive strength testing was also conducted on core samples obtained from the soil cement columns in the test plot, taken 28 days after construction. The samples with diameter of 60 mm and height of 120 mm were taken at every 1 m depth to 5 m.
The results showed that the unconfined compressive strength of core samples obtained from the test plot ranged from 0.92 MPa to 2.34 MPa with an average of 1.56 MPa, generally appropriate for the compressive strength of soil cement columns (Mun et al., 2012). In addition, the secant modulus (E50) ranged from 63.31 MPa to 214.63 MPa with an average of 133.32 MPa, which corresponded to the results of Lorenzo and Bergado., (2006) at 60.50 MPa to 122.00 MPa. The relationship between the unconfined compressive strength and secant modulus (E_{50}) is shown in **Fig. 4** (Jamsawang et al., 2015). This was used to estimate the stress - strain for numerical modeling in earth excavations (Mun et al., 2012).

3.2 Shear interface between soil cement and H-shaped steel

The H-shaped steel was embedded in the soil cement columns and tests were conducted by pushing the H-shaped steel through the surrounding soil cement and shear interface as determined from Equation 1 as,

$$\tau_{inter} = \frac{F}{(P_{steel})L_{steel}} \quad [1]$$

where τ_{inter} = shear interface (kPa),
F = vertical force (kN),
P_{steel} = perimeter of steel (m), and
L_{steel}= embedded length of H-shaped steel in the soil cement column (m).

Two types of model test were prepared namely: (1) soil cement column of diameter 0.35 m and 0.50 m height with embeded 100x100 mm H-shaped steel, and (2) soil cement column of diameter 0.40 m and 0.50 m with embedded 125x125 mm H-shaped steel. Each sample contained soil cement with different unconfined compressive strength. The test set up is shown in **Fig**. **5**. The H-steel embedded into the core of the soil cement was produced according to TIS 1227-1996, SS400. The characteristics of the H-steel are shown in **Table 2**.

Test results showed that the unconfined compressive strength of the cement column had an influence on shear interface between the H-shaped steel and soil cement. The greater the unconfined compressive strength, the higher the shear interface obtained. The shear interface between 100x100 mm H-shaped steel and soil cement was 39.79 kPa, and 49.04 kPa for unconfined compressive strengths of soil cement at 711.92 kPa and 1671.05 kPa, respectively, as shown in **Fig**. **6**. The shear interface between 125x125 mm H-shaped steel and soil cement was 26.54 kPa, and 44.75 kPa, for unconfined compressive strength of soil cement at 575.65 kPa and 1513.17 kPa, respectively, as shown in **Fig**. **7**. As a consequence, the interface friction coefficient, (R_{inter}) was obtained from Equation 2 as,

$$R_{inter} = \frac{\tau_u}{q_u} \quad [2]$$

where τ_{inter} = interface friction coefficient
τ_u = ultimate shear interface (kPa), and
q_u = unconfined compressive strength of soil cement (kPa).

In this study, the Rinter of steel embedded in the soil cement mixture ranged from 0.03 to 0.05, less than that of concrete embedded soil cement, due to slippage on the smooth surface of the steel. However, the Rinter of concrete embedded soil cement ranged from 0.348 to 0.426 (Voottipruex et al., 2010) due to the rough surface of the concrete piles.

3.3 Flexural strength test of the embedded soil cement column

The soil cement columns were cast with diameter of 0.25 m and height of 1.0 m, reinforced with 50x50 mm fabricated H-shaped steel. Flexural strength tests were conducted after the specimens were cured at room temperature for 28 days. The soil cement reinforced with H-shaped steel resisted flexural stress in an elastic range as shown in **Fig**. **8**. Maximum flexural stress was recorded at 11.71 kPa and gradually decreased to a certain level with simultaneous increase due to H-shaped steel reinforcement. Beyond the elastic range, the maximum flexural strength was 30.15 kPa and this decreased due to the ultimate failure of soil cement reinforced with H-shaped steel.

4. Soil cement wall test plots

4.1 Types of soil cement wall

Soil cement walls are used for excavation control, to stabilize open cuts and protect structures with shallow foundations surrounding the excavation, and as a measure against seepage. Walls can be constructed with tangential or overlapping elements. Overlapping is particularly important when executing cut-off walls or environmental barriers (Topolnicki, 2004).In this study soil cement columns were constructed in the test plot using a jet grouting method with diameter of 0.60 m and overlapped by 0.10 m to form 4.60 m length walls. There were five patterns of soil cement wall.

Type A consisted of three consecutive rows of soil cement columns with effective thickness of 1.33 m. Type B consisted of two consecutive rows of soil cement columns with effective thickness of 0.83 m. Type C consisted of one consecutive row of soil cement columns with effective thickness of 0.33 m. The 200x200 mm H-shaped steel of 6 m length was inserted in every soil cement column of type C. Type D was similar to type C, except that 200x200 mm H-shaped steel of 6 m length was inserted alternatively in the soil cement columns. Type E consisted of one consecutive row of soil cement columns with effective thickness of 0.33 m without steel reinforcement as shown in **Fig. 9**.

Soil cement columns were constructed in the field using a jet grouting method with diameter of 600 mm and overlapped by 100 mm to form 4.60 m length walls. There were five patterns of soil cement wall as shown in Fig. 9 .While surface settlement plates and Inclinometer were installed as shown in **Figs. 10** and **11**.

4.2 Horizontal movement of soil cement wall

Excavation was conducted down to 5 m depth for each type of soil cement wall and horizontal movement was measured. The results are shown in **Fig**. **12**. Type A wall exhibited horizontal movement of 6.37 mm, while types B, C, and D exhibited horizontal movement of 15.76, 22.37, and 51.99 mm, respectively. In contrast, failure was determined for type E soil cement wall as shown in **Fig**. **13**.

Considering the ratio between the excavation depth and effective thickness of all types of wall, Borges et al. (2013) defined the effective thickness as shown in **Fig**. **14**. To reduce construction area, soil cement walls with H-shaped steel reinforcement can replace soil cement walls without reinforcement which thickness is required. The relationship between excavation depth, effective thickness ratio, and horizontal displacement is shown in **Fig**. **15**. Type C wall with effective thickness of 0.33 m

Fig. 3. Strain measurements by affixing strain gauge on steel surface.

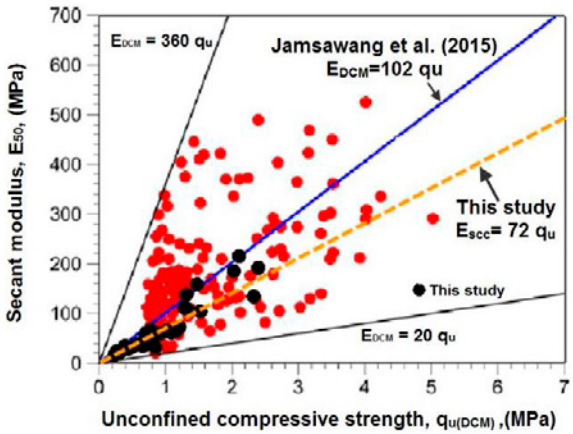

Fig. 4. Relationship between the unconfined compressive strength and secant modulus (E_{50}) (Jamsawang et al., 2015 and this study).

Table 2. Characteristics of the H-steel for shear interface tests.

Dimension (mm)	Weight (kg/m)	Cross section ($x10^{-3}$ m^2)	Moment of Inertia ($x10^{-6}$ m^4)		Section modulus ($x10^{-4}$ m^3)	
			I_x	I_y	Z_x	Z_y
125x125	23.80	3.031	8.47	2.93	1.36	0.47
100x100	17.20	2.190	3.83	1.34	0.77	455

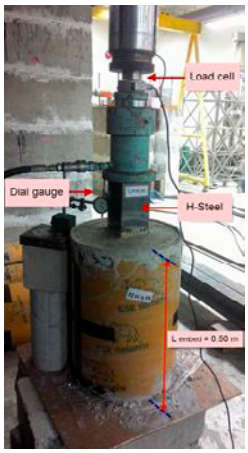

Fig. 5. Test set up of shear interface.

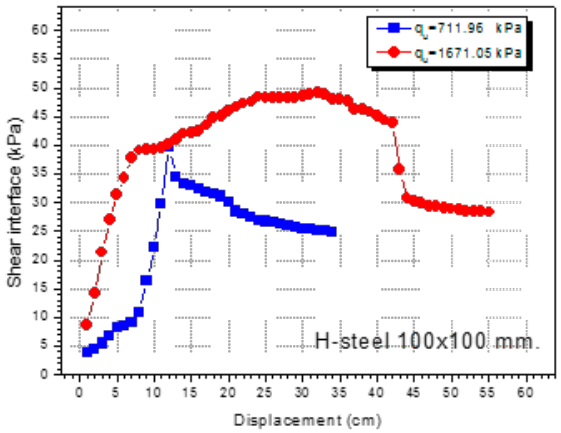

Fig. 6. Relationship between displacement and shear interface of 100x100 mm H-shaped steel.

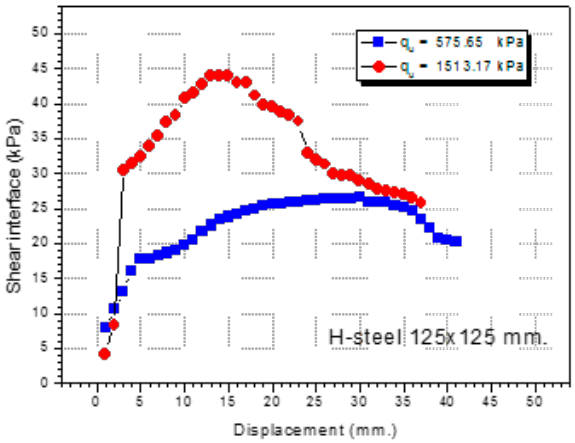

Fig. 7. Relationship between displacement and shear interface of 125x125 mm H-shaped steel.

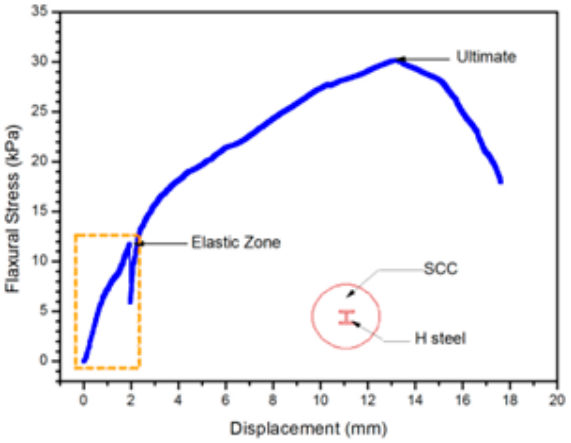

Fig. 8. Relationship between vertical displacement and flexural stress of the embedded soil cement column.

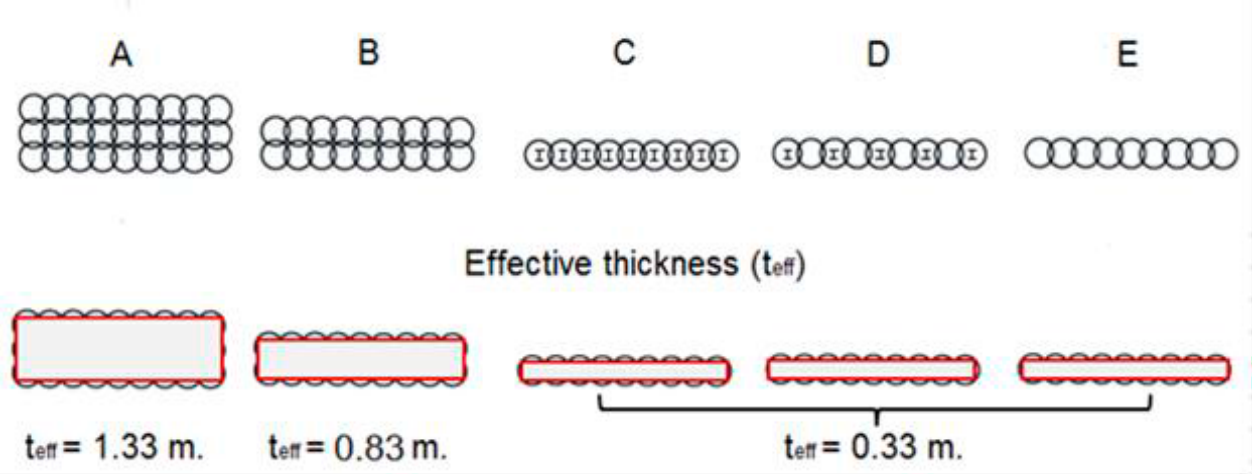

Fig. 9. Five patterns of soil cement wall and effective thickness.

exhibited maximum horizontal displacement of 15 mm, while type D wall showed a horizontal displacement of 37 mm. Type B wall with effective thickness of 0.83 m exhibited maximum horizontal displacement of about 10

Fig. 10. Installation of the inclinometer with diameter of 70 mm.

Fig. 11. Installation of the surface settlement plate behind the soil cement wall.

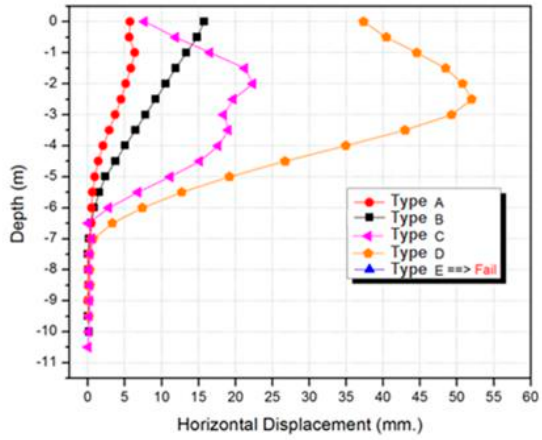

Fig. 12. Horizontal lateral movement of soil cement wall at excavation depth of 5 m.

Fig. 13. Failure of type E soil cement wall at excavation depth of 5 m.

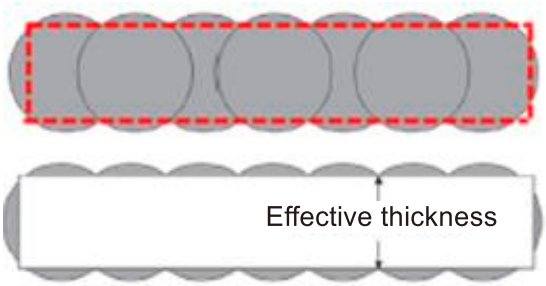

Fig. 14. Effective thickness of soil cement wall (Borges et al., 2013).

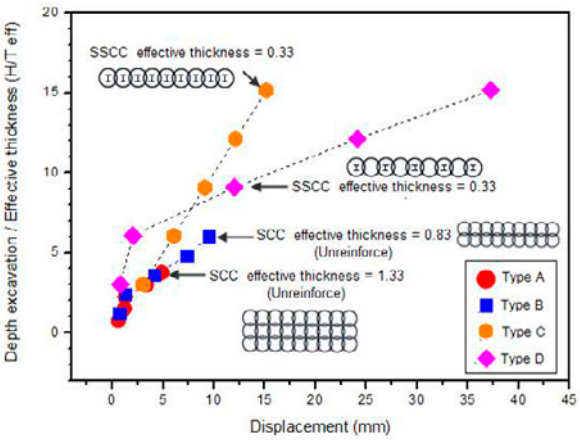

Fig. 15. Relationship between excavation depth to effective thickness ratio, and horizontal displacement.

mm, and type A wall with effective thickness of 1.33 m exhibited maximum horizontal displacement of 5 mm. Results implied that wall thickness and movement could be reduced by embedding H-shaped steel, and less area was also required.

Table 2. Characteristics of the H- steel for shear interface tests.

Dimension (mm)	Weight (kg/m)	Cross section ($x10^{-3}$ m^2)	Moment of Inertia ($x10^{-6}$ m^4)		Section modulus ($x10^{-4}$ m^3)	
			I_x	I_y	Z_x	Z_y
125x125	23.80	3.031	8.47	2.93	1.36	0.47
100x100	17.20	2.190	3.83	1.34	0.77	455

4.3 Strain measurement on the steel surface

Strain gauges were calibrated in the laboratory prior to installation to derive an equation relating strain and displacement for the particular gauge and appropriate weatherproofing material were affixed on the H-shaped steel surface every 1 m prior to insertion in the soil cement wall. In order to record strain on the H-shaped steel surface. The 0.60 m diameter soil cement column was constructed consecutively in a single row with 0.10 m column overlap. The 200x200 mm H-shaped steel of 6 m length was inserted in type C and D soil cement column wall. The type C wall was a single row cement column with H- steel reinforcement in every column, while type D wall was a single row cement column with alternate H-shaped steel reinforcement. During excavation, strain was detected until 5 m depth was reached.

Figure 16 shows strain measurements from strain gauges affixed on the steel surface of type C cement column wall. At 1 m excavation, the maximum strain obtained at the ground surface of 40 με and the minimum strain of 15 με was obtained at 6 m depth. At 2 m excavation, the maximum strain obtained at 2 m depth of 50 με and the minimum strain of 30 με was obtained at 6 m depth. At 3 m excavation, the maximum strain obtained at 3 m depth of 70 με and the minimum strain of 50 με was obtained at 6 m depth. At 4 m excavation, the maximum strain obtained at 4 m depth of 80 με and the minimum strain of 50 με was obtained at 6 m depth. At 5 m excavation, the maximum strain obtained at 5 m depth of 170 με and the minimum strain of 100 με was obtained at 6 m depth. It can be concluded that the maximum strain in each excavation depth was obtained at that depth while the minimum was obtained at 6 m depth.

Figure 17 shows strain measurements from strain gauges affixed on the steel surface of type D cement column wall. At 1 m excavation, the maximum strain obtained at 1 m depth the ground surface of 50 με and the minimum strain of 5με was obtained at 6 m depth. At 2 m excavation, the maximum strain obtained at 2 m depth of 80 με and the minimum strain of 10με was obtained at 3 m depth. At 3 m excavation, the maximum strain obtained at 3 m depth of 100 με and the minimum strain of 25 με was obtained at ground surface. At 4 m excavation, the maximum strain obtained at 4 m depth of 275 με and the minimum strain of 20 με was obtained at 2 m depth. At 5 m excavation, the maximum strain obtained at 5 m depth of 80 με and the minimum strain of 10 με was obtained at 6 m depth. It can be concluded that the maximum strain was obtained at 4 m depth. Comparing between these types of soil cement wall, the type C wall is more rigid than the type D wall. The maximum strain obtained from type C wall is much less than the type D wall in every excavation depth.

.

4.4 Bending moment during excavation

Figure 18 shows the strain detected from the H-shaped steel surface of 200x200 mm in an elastic range. The maximum bending moment was calculated from Equations 3 and 4 at each depth. Equations based on the usual elastic assumptions: Stress is proportional to strain, a plane section before bending remains a plane section after bending (Mc Cormac et al., 2012), while the minimum was scattered due to alternate reinforcement.

Comparing the types of soil cement wall, type C wall was more rigid than type D. The maximum strain obtained from type C wall was much less than from type D wall at every excavation depth as shown in **Figs. 16** and **17** respectively.

$$\sigma_s = E_s \times \varepsilon_s \quad [3]$$

$$M_n = \sigma_s \times Z_x \quad [4]$$

where

Mn = maximum bending moment (kN-m),

σ_s = stress (kPa),

Zx = section modulus of H-shaped steel,

E_s = modulus of elasticity of H-shaped steel = 235.36 MPa, and

ε_s = the measured strain from the strain gauge.

The H-shaped steel embedded into the core of the soil cement column was produced according to TIS 1227-1996, SS400. The characteristics of the H-shaped steel are shown in **Table 3**.

Regarding to Equations 3 and 4, most of the maximum bending moment occurred at excavation depth. For type D wall, the maximum moment occurred at 4 m of excavation depth as 25.41 kN-m. At 5 m excavation depth the maximum bending moment decreased to 8.26 kN-m as shown in **Fig. 20**. The alternate H-shaped steel reinforcement, type C endured bending moment due to lateral earth pressure up to a certain excavation depth and its movement was in bending mode. Beyond this

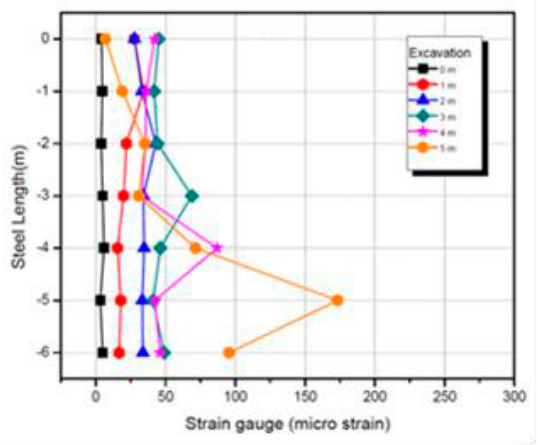

Fig. 16. Measured strain on steel surface of type C cement column during shallow excavation.

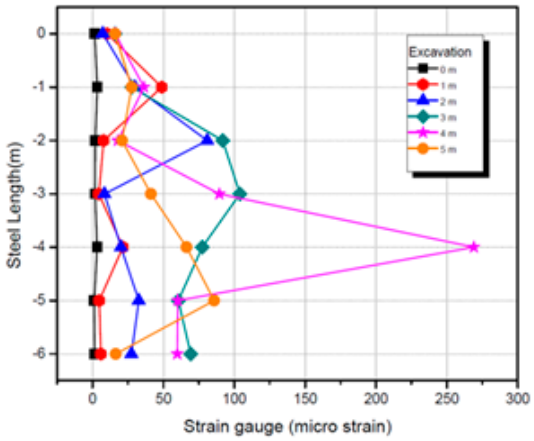

Fig. 17. Measured strain on steel surface of type D cement column during shallow excavation.

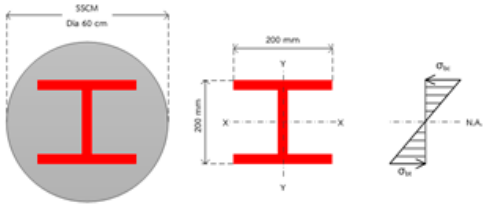

Fig. 18. Bending moment in the elastic range of H-shaped steel.

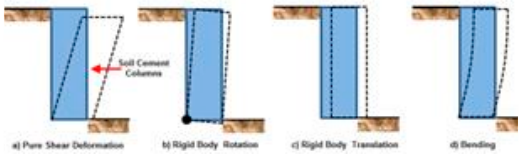

Fig. 19. Horizontal movement mode of a soil cement wall (Briaud et al., 2000; Mun et al., 2012).

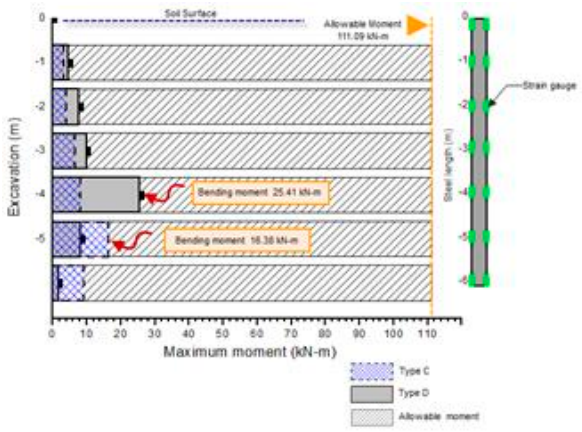

Fig. 20. Bending moment for embedded H-shaped steel compared to allowable values.

Fig. 21. Horizontal load test setup.

depth the bending moment decreased and the horizontal movement of the wall was in rigid body translation mode. The modes of horizontal movement of a soil cement wall are shown in **Fig. 19**. For type D wall, the bending moment increased as the excavation depth increased, and the maximum occurred at 5 m depth as 16.38kN-m.as shown in **Fig. 20**.

Comparisons were made between the type C, D, and E soil cement walls. The soil cement walls resisted bending moment due to lateral earth pressure through the H-shaped steel embedded in the soil cement columns. The maximum bending moment occurred in type D wall as higher than type C wall because the embedded distance of the H-shaped steel in type D wall was two times larger than in type C wall. According to the Thai Industrial Standards (TIS), the allowable maximum bending moment of shaped steel is 235.36 MPa. The bending moment in embedded H-shaped steel in type C, and D walls obtained from Equations 3 and 4 was less than the allowable value, as shown in **Fig. 20**.

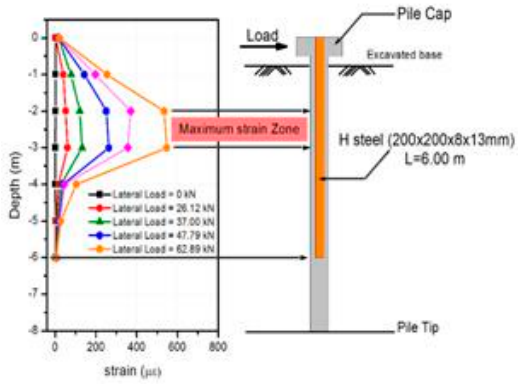

Fig. 22. Relationship between depth and strain along the embedded steel during the horizontal movement test.

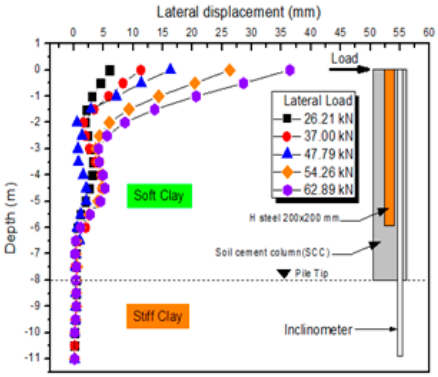

Fig. 23. Relationship between depth and horizontal displacement due to horizontal force applied at the top of the test pile.

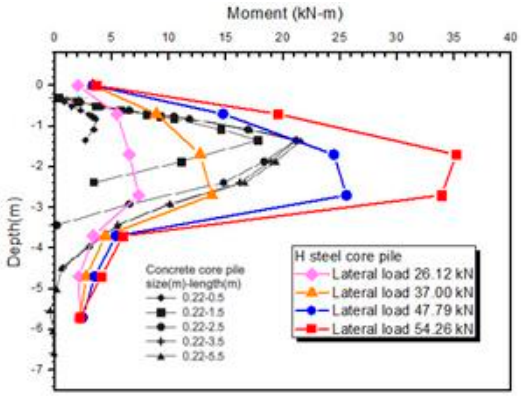

Fig. 24. Relationship between horizontal load and horizontal displacement.

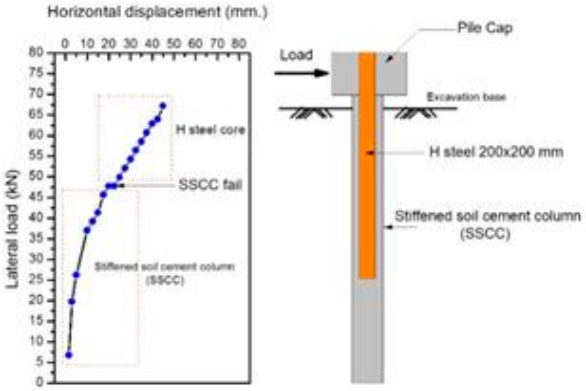

Fig. 25. Embedded H-shaped steel.

4.5 Horizontal movement of single pile

The test was conducted on the pile cap of the stiffened soil cement column constructed in the test plot. The test setup is shown in **Fig**. **21**. An H-shaped steel with depth and width of 200 mm, web thickness of 8 mm and flange thickness of 12 mm (H-200×200×8×12 mm) was embedded into the soil cement column. As the strain was detected, it indicated that lateral force was transferred to the embedded steel. **Fig. 22** shows the relationship between excavation depth and strain affixed on the pile cap. The horizontal movement at the pile cap increased as the lateral force increased. The maximum lateral movement with depth was 36.43 mm with lateral force of 62.89 kN as illustrated in **Fig. 23**.

The test was conducted until loading increment slightly increased or remained constant. The ultimate horizontal force applying for SSCC was observed at 47.79 kN. Beyond this point the SSCC continuously resisted the horizontal force through the embedded H-shaped steel which was able to resist horizontal load.

Therefore, the stability of the wall still remains as a consequence. The relationship between horizontal load and the horizontal displacement is shown in **Fig. 24**.

Voottipruex et al. (2010) studied SSCC embedded by 6 m length of 15 cm diameter hollow core concrete piles. The maximum bending moment was observed at 0.80 m depth from the ground surface, while it was observed at between 1.0 to 2.0 m from the ground surface in this research as shown in **Fig. 25**.

5. Conclusions

From the laboratory test results and shallow excavation of the soil cement walls in the field test, the following conclusions were drawn.

1. The empirical relation between the modulus of elasticity and the unconfined compressive strength relate to secant modulus (E_{50}) obtained from this study was equal to 72 q_u, corresponding to findings by Jamsawang et al., (2015) which indicated that the secant modulus (E_{50}) was in the range of 20 q_u to 360 q_u.
2. From the laboratory tests, the results revealed that there was shear interface between the embedded steel and unconfined compressive strength. Two types of H-shaped steel were used namely: 100×100 mm with surface area of 0.285 m^2 and 125×125 mm with surface area of 0.36 m^2. The former was embedded in soil cement columns with unconfined compressive strength of 711.92 kPa and 1671.05 kPa, and the shear interfaces obtained were 39.79 kPa and 49.04 kPa, respectively. The latter was embedded in soil cement columns with unconfined compressive strength of 575.50 kPa and 1513.17 kPa, and the shear interface obtained was 26.54 kPa and 44.75 kPa, respectively. The higher the unconfined compressive strength the higher the shear interface obtained. The interface friction coefficient (R_{inter}) was in the range 0.03 to 0.05.
3. The relationship between excavation depth to effective thickness ratio (H/T_{eff}) have an effect on horizontal displacement of soil cement column wall .The horizontal movement of the wall less than 15 mm Type C is one row of cement column inserted with H-shaped steel in each column could be replace to Type A(three row without reinforcement) and Type B(two row without reinforcement) so that reduce area of excavation support systems are temporary earth retaining structures
4. The alternate H-shaped steel reinforcement in type D wall resisted bending moment due to lateral earth pressure up to certain excavation depths and movement was in bending mode. Beyond this depth, the bending moment decreased and the horizontal movement of the wall was in rigid body translation mode. The SSCC wall resisted bending moment due to lateral earth pressure through the embedded H-shaped steel in the soil cement columns.
5. The detected strain indicated that horizontal force was transferred to the embedded steel. The horizontal movement at the pile cap increased as horizontal force increased. The SSCC continuously resisted the horizontal force through the embedded H-shaped steel, and a linear relationship between the horizontal load and horizontal displacement was observed.

Acknowledgements

The authors would like to thank the National Research Council and King Mongkut's University of Technology North Bangkok for their financial support of this research

References

Bergado, D.T., Anderson, L.R. and Miura, N., Balasubramaniam, A.S., 1996. Soft ground improvement. New York: ASCE Press: 241-243.

Bergado, D.T., Lorenzo, G.A. and Abuel-naga, H.M., 2004. Fundamentals of thermal and cement stabilization. Proc. International Symposium on Lowland Technology (ISLT 2004), September 1-3, 2004, Bangkok, Thailand: 85-94.

Borges, J.L. and Guerra, G.T., 2003. Cylindrical excavations in clayey soils retained by jet grout walls: Numerical analysis and parametric study considering the influence of consolidation. Computers and Geotechnics, **55**: 42-56.

Briaud, J.L., Nicholson, P. and Lee, J., 2000. Behavior of full-scale vert wall in sand. J. Geotech. and Geoenv. Engrg., **126** (9): 808-818.

Boathong, P., Mairaing, W. and Jamsawang, P., 2014. Lateral movement of slope stabilized with DCM column rows. Electronic J. Geotech. Engrg., **19**: 1647-1664.

Jamsawang, P., Voottipruex, P., Jongpradist, P. and Bergado, D.T., 2015. Parameters affecting the lateral movements of compound deep cement mixing walls by numerical simulations and parametric analyses. Acta Geotechnica: 797-812.

Han, J., 2015. Principles and practice of ground improvement. John Wiley and Son Inc., New Jersey: pp 252.

Lorenzo, G.A., Bergado, D.T. and Soralump, S., 2006. New and economical method of cement admixed clay for DMM application. Geotechnical Testing Journal, **29**: 54-63.

Lorenzo, G.A. and Bergado, D.T., 2006. Fundamental characteristics of cement-admixed clay in deep mixing. J. Materials in Civil Engrg., **18**: 161-174.

Mun, B., Kim, T., Moon,T. and Oh, J. 2012. SCM wall in sand : Numerical simulation and design implication. Engineering Geology, **151**: 15-23.

Modoni, G. and Bzówka, J., 2012. Analysis of foundations reinforced with jet grouting. J. Geotech. Geoenviron. Engrg., **138** (12): 1442-1454.

Mc.Cormac, J.C. and Csernak, S.F., 2012. Structural steel design, Pearson Education, Harlow, England, Fifth Eds.: pp. 250.

Porbaha, A., Zen, K. and Kobayashi, M., 1999. Deep mixing technology for liquefaction mitigation. J. Infrastructure Systems, **5**: 21-34.

Topolnicki, M., 2004. In situ soil mixing. Ground Improvement, Moseley, M.P. and Kirsch, K. (Editors), Spon press, Second Eds.: 331-423.

Voottipruex, P., Suksawat, T. and Jamsawang, P., 2010. Numerical simulations and parametric study of SDCM and DCM piles under full scale axial and lateral loads. Computers and Geotechnics, **38**: 318-329.

Wang, S. and Cao, B., 2008. Experimental study on interaction mechanism of small H-beams and a soil-cement retaining wall. J. China Univ Mining&Technol, **18** (1): 149-152.